Electron-Transfer Processes in Metal-Free Tetraferrocenylporphyrin. Understanding Internal Interactions To Access Mixed-Valence States Potentially Useful for Quantum Cellular Autom...

12 AUTHORS, INCLUDING:

Victor N Nemykin
University of Minnesota Duluth
202 PUBLICATIONS **2,601** CITATIONS

SEE PROFILE

Pierluca Galloni
University of Rome Tor Vergata
46 PUBLICATIONS **672** CITATIONS

SEE PROFILE

Barbara Floris
University of Rome Tor Vergata
95 PUBLICATIONS **1,194** CITATIONS

SEE PROFILE

Robertino Zanoni
Sapienza University of Rome
142 PUBLICATIONS **1,901** CITATIONS

SEE PROFILE

Electron-Transfer Processes in Metal-Free Tetraferrocenylporphyrin. Understanding Internal Interactions To Access Mixed-Valence States Potentially Useful for Quantum Cellular Automata

Victor N. Nemykin,*,† Gregory T. Rohde,† Christopher D. Barrett,† Ryan G. Hadt,†
Claudia Bizzarri,†,‡ Pierluca Galloni,*,‡ Barbara Floris,‡ Israel Nowik,§
Rolfe H. Herber,*,§ Andrea G. Marrani,‖ Robertino Zanoni,‖ and Nikolay M. Loim⊥

*Department of Chemistry & Biochemistry, University of Minnesota−Duluth,
Duluth, Minnesota 55812, Dipartimento di Scienze e Tecnologie Chimiche, Università di Roma
"Tor Vergata", via della ricerca scientifica, 00133 Rome, Italy, Racah Institute of Physics, The
Hebrew University of Jerusalem, 91904 Jerusalem, Israel, Dipartimento di Chimica, Università
degli Studi di Roma "La Sapienza", p.le Aldo Moro 5, 00185 Rome, Italy, and A. N.
Nesmeyanov Institute of Organoelement Compounds, 28 Vavilov Street, 117813 Moscow, Russia*

Received July 1, 2009; E-mail: vnemykin@d.umn.edu; galloni@scienze.uniroma2.it; herber@vms.huji.ac.il

Abstract: Redox properties of H_2TFcP [$TFcP^{2-}$ = 5,10,15,20-tetraferrocenylporphyrin(2−)] were investigated using cyclic voltammetry, differential pulse voltammetry, and square-wave voltammetry methods in a large variety of solvents and electrolytes. When DMF, THF, and MeCN were used with TBAP as the supporting electrolyte, the first oxidation wave was assigned to a single four-electron oxidation process reflecting simultaneous oxidation of all iron(II) centers into iron(III) centers in H_2TFcP. When an o-DCB (1,2-dichlorobenzene)/TBAP combination was used in electrochemical experiments, four ferrocene substituents underwent two very diffuse, "two-electron" stepwise oxidations. The use of a weakly coordinating TFAB ($[NBu_4][B(C_6F_5)_4]$) electrolyte in o-DCB or DCM results in four single-electron oxidation processes for ferrocene substituents in which the first and second single-electron waves have a relatively large separation, while the second, third, and fourth oxidation processes are more closely spaced; similar results were observed when a DCM/TBAP system and an imidazolium cation-based ionic liquid (($bmim$)Tf_2N = N-butyl-N'-methylimidazolium bis(trifluoromethanesulfonyl)imide) were used. Spectroelectrochemical oxidation of H_2TFcP in o-DCB or DCM with TFAB as the supporting electrolyte allowed for characterization of the mixed-valence $[H_2TFcP]^+$, $[H_2TFcP]^{2+}$, and $[H_2TFcP]^{3+}$ compounds by UV−vis spectroscopy in addition to the "all-Fe^{III}" $[H_2TFcP]^{4+}$. The chemical oxidation of H_2TFcP was tested using a variety of oxidants which resulted in formation of mixed-valence $[H_2TFcP]^+$ and $[H_2TFcP]^{2+}$ as well as $[H_2TFcP]^{4+}$, which were characterized by UV−vis−NIR, MCD, IR, Mössbauer, and XPS spectroscopy. The intervalence-charge-transfer bands observed in the near-IR region in $[H_2TFcP]^+$ and $[H_2TFcP]^{2+}$ complexes were analyzed using Hush formalism and found to be of class II (in Robin−Day classification) character with localized ferrous and ferric centers. Class II behavior of $[H_2TFcP]^+$ and $[H_2TFcP]^{2+}$ complexes was further confirmed by Mössbauer, IR, and XPS data.

Introduction

Transition-metal-containing compounds with a strong long-range metal−metal coupling represent an important class of metallocomplexes.[1] These molecules were intensely studied because of their interesting fundamental properties (i.e., multiredox processes, magnetic coupling, and unpaired electron

density migration). Such nanomeric size multinuclear switchable arrays are also interesting from the practical (i.e., molecular electronics, quantum cellular automata, optoelectronic materials for application in high-speed photonic or redox devices) point of view.[2,3] In all cases, formation of the mixed-valence (MV) states in polynuclear transition-metal complexes, particularly those containing ferrocene, are responsible for the above-mentioned properties.[3] The multinuclear ferrocene derivatives with MV states have been known for many years, and the factors affecting their formation and stability have been thoroughly investigated.[4] In most cases, iron centers should be located at a

† University of Minnesota−Duluth.
‡ Università di Roma "Tor Vergata".
§ The Hebrew University of Jerusalem.
‖ Università degli Studi di Roma "La Sapienza".
⊥ A. N. Nesmeyanov Institute of Organoelement Compounds.
 (1) (a) Kaim, W.; Lahiri, G. K. *Angew. Chem., Int. Ed.* **2007**, *46*, 1778. (b) Kaim, W.; Sarkar, B. *Coord. Chem. Rev.* **2007**, *251*, 584. (c) Chisholm, M. H.; Patmore, N. J. *Acc. Chem. Res.* **2007**, *40*, 19. (d) Solomon, E. I.; Sarangi, R.; Woertink, J. S.; Augustine, A. J.; Yoon, J.; Ghosh, S. *Acc. Chem. Res.* **2007**, *40*, 581.

 (2) (a) Miller, J. S.; Epstein, A. J. *Angew. Chem., Int. Ed.* **1994**, *33*, 385. (b) Epstein, A. J.; Miller, J. S. *Synth. Met.* **1996**, *80*, 231. (c) Barlow, S. *Inorg. Chem.* **2001**, *40*, 7047.
 (3) Barlow, S.; O'Hare, D. *Chem. Rev.* **1997**, *97*, 637.

distance of less than 5−6 Å to achieve effective metal−metal coupling between ferrocene units in the same molecule, while examples of long-range (∼10 Å) metal−metal couplings in polyferrocenyl-containing systems are still rare.[5−11]

In 1999, Barrell et al. showed a rare example of a pure atropisomer formation for the α,α−5,15-bisferrocenyl-2,8,12,18-tetrabutyl-3,7,13,17-tetramethylporphyrin, which demonstrated a long-range (>10 Å) metal−metal coupling between two ferrocenyl substituents.[5] The same long-range metal−metal coupling and macrocycle metal dependence was later observed for a very similar compound, α,α−5,15-bisferrocenyl-2,8,12,18-tetrabutyl-3,7,13,17-tetraethylporphyrin.[6] Both research teams have reasonably suggested that the probable reason for the observed metal−metal interactions is due to restricted conformational flexibility of ferrocene groups, because when ferrocenyl groups are conformationally flexible as in 5,15-diferrocenyl-10,20-di-*p*-tolylporphyrin, no metal−metal coupling is observed in electrochemical and spectroelectrochemical experiments conducted using a DCM/TBAP system.[5] In accord with this hypothesis, other *meso*-tetraferrocenylporphyrin systems, with the ferrocenyl units connected to the porphyrin core through aromatic linking groups, were reported to be unable to form MV complexes.[12]

meso-Ferrocenyl-substituted porphyrins with direct porphyrin−ferrocene C−C bonds have received relatively scarce attention, although they seem very promising in terms of photochemical properties and application in molecular electronics.[9,10,13,14] A reason for the lack of investigation until recently may be the difficulty of finding a synthetic method for pure ferrocenylporphyrins. In fact, contradictory results in terms of MV species formation may or may not be related to the purity of the compounds. The first 5,10,15,20-tetraferrocenylporphy-

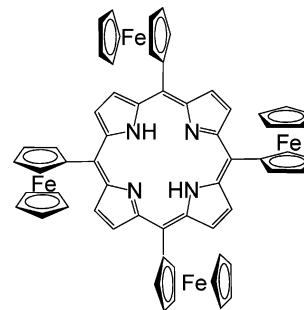**Figure 1.** Structure of H₂TFcP.

rins, MTFcP (M = H₂, Cu, Zn), were described in 1977,[15] but the unacceptably low purity of the compounds raised doubts in the reported formation of the MV derivatives of MTFcP. The synthesis of pure H₂TFcP and its transition-metal complexes had not been published until recently and allowed us to obtain target compounds in relatively high yield and purity.[9,16] Several years later, another team of researchers proposed an alternative synthetic route for the preparation of MTFcP compounds and supported Burrell's hypothesis about simultaneous oxidation of all four ferrocene substituents in MTFcP at the same potential.[17] These data, however, were in disagreement with our preliminary results on the chemical oxidation of MTFcP complexes[10] and stimulated us to carefully investigate redox properties of H₂TFcP and its transition-metal complexes especially taking into consideration the unusual photochemical properties of ZnTFcP in a supramolecular system with fullerene and indications of the formation of the MV states in H₂TFcP and bisferrocenylbisphenylporphyrins.[7,9] In our previous paper, we presented the preparation and characterization of neutral H₂TFcP and MTFcP (M = Co, Ni, Cu, and Zn) complexes.[8] Understanding the electronic origins of the tetraferrocenylporphyrin properties is necessary to exploit them for practical purposes. The quest for such a complete understanding led us to conduct an accurate electrochemical investigation with different electrolytes and a wide range of solvents, among which are ionic liquids, rarely used as electrochemical solvents.[18] The formation, characterization, and stability of chemically or electrochemically generated MV states in H₂TFcP (Figure 1) are discussed in the current paper. Several MV species were identified and characterized using UV−vis, MCD, IR, XPS, and Mössbauer spectroscopy.

Results and Discussion

Electrochemistry of H₂TFcP. The influence of the solvent/electrolyte combination as well as statistical, magnetic inductive, electrostatic, and electronic coupling factors on electron-transfer processes and $\Delta E_{1/2}$ values in the multinuclear transition-metal complexes is well-discussed in the literature.[19] In particular, it was suggested that the best solvent/electrolyte combination for the investigation of polyferrocenyl-containing complexes should consist of a low-polarity solvent and a noncoordinating electrolyte.[19] Thus, following ideas developed by Geiger et al.,[19] the redox behavior of H₂TFcP was investigated by cyclic voltammetry (CV), differential pulse voltammetry (DPV), and

(4) (a) Cowan, D. O.; Kaufman, F. *J. Am. Chem. Soc.* **1970**, *92*, 6198. (b) Cowan, D. O.; Kaufman, F. *J. Am. Chem. Soc.* **1970**, *92*, 219. (c) Morrison, W. H., Jr.; Hendrickson, D. N. *Chem. Phys. Lett.* **1973**, *22*, 119. (d) Morrison, W. H.; Krogsrud, S.; Hendrickson, D. N. *Inorg. Chem.* **1973**, *12*, 1998. (e) Morrison, W. H., Jr.; Hendrickson, D. N. *Inorg. Chem.* **1975**, *14*, 2331. (f) Dong, T. Y.; Hendrickson, D. N. *Bull. Inst. Chem., Acad. Sin.* **1987**, *34*, 67. (g) Tolbert, L. M.; Zhao, X.; Ding, Y.; Bottomley, L. A. *J. Am. Chem. Soc.* **1995**, *117*, 12891. (h) Ribou, A.-C.; Launay, J.-P.; Sachtleben, M. L.; Li, H.; Spangler, C. W. *Inorg. Chem.* **1996**, *35*, 3735. (i) Patoux, C.; Coudret, C.; Launay, J.-P.; Joachim, C.; Gourdon, A. *Inorg. Chem.* **1997**, *36*, 5037. (j) Hadt, R. G.; Nemykin, V. N. *Inorg. Chem.* **2009**, *48*, 3982.

(5) Burrell, A. K.; Campbell, W. M.; Jameson, G. B.; Officer, D. L.; Boyd, P. D. W.; Zhao, Z.; Cocks, P. A.; Gordon, K. C. *Chem. Commun.* **1999**, 637.

(6) Rhee, S. W.; Na, Y. H.; Do, Y.; Kim, J. *Inorg. Chim. Acta* **2000**, *309*, 49.

(7) Auger, A.; Swarts, J. *Organometallics* **2007**, *26*, 102.

(8) Nemykin, V. N.; Galloni, P.; Floris, B.; Barrett, C. D.; Hadt, R. G.; Subbotin, R. I.; Marrani, A. G.; Zanoni, R.; Loim, N. M. *Dalton Trans.* **2008**, 4233.

(9) Nemykin, V. N.; Barrett, C. D.; Hadt, R. G.; Subbotin, R. I.; Maximov, A. Y.; Polshin, E. V.; Koposov, A. Y. *Dalton Trans.* **2007**, 3378.

(10) Nemykin, V. N.; McGinn, M.; Koposov, A. Y.; Tretyakova, I. N.; Polshin, E. V.; Loim, N. M.; Abramova, N. V. *Ukr. Khim. Zh.* **2005**, *71*, 79.

(11) Nemykin, V. N.; Kobayashi, N. *Chem. Commun.* **2001**, 165.

(12) (a) Cheng, K.-L. C.; Li, H.-W.; Ng, D. K. P. *J. Organomet. Chem.* **2004**, *689*, 1593. (b) Hodgson, M. C.; Burrell, A. K.; Boyd, P. D. W.; Brothers, P. J.; Rickard, C. E. F. *J. Porphyrins Phthalocyanines* **2002**, *11*, 737. (c) Poon, K. W.; Liu, W.; Chan, P. K.; Yang, Q.; Chan, T. W. D.; Mak, T. C. W.; Ng, D. K. P. *J. Org. Chem.* **2001**, *66*, 1553.

(13) (a) Gostev, F. E.; Nadtochenko, V. A.; Sarkisov, O. M.; Loim, N. M.; Abramova, N. V.; Chirvonyi, V. S. *Khim. Fiz.* **2004**, *23*, 3. (b) Nadtochenko, V. A.; Denisov, N. N.; Gak, V. Y.; Abramova, N. V.; Loim, N. M. *Russ. Chem. Bull.* **1999**, *148*, 1900.

(14) Galloni, P.; Floris, B.; De Cola, L.; Cecchetto, E.; Williams, R. M. *J. Phys. Chem. C* **2007**, *111*, 1517.

(15) Wollmann, R. G.; Hendrickson, D. N. *Inorg. Chem.* **1977**, *16*, 3079.

(16) Loim, N. M.; Abramova, N. V.; Sokolov, V. I. *Mendeleev Commun.* **1996**, *6*, 46.

(17) Narayanan, S. J.; Venkatraman, S.; Dey, S. R.; Sridevi, B.; Anand, V. R. G.; Chandrashekar, T. K. *Synlett* **2000**, 1834.

(18) Wasserscheid, P.; Welton, T., Eds. *Ionic Liquids in Synthesis*, 2nd ed.;Wiley-VCH: New York, 2008.

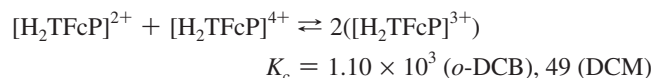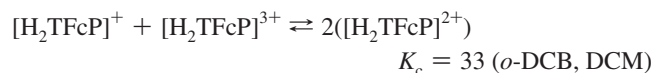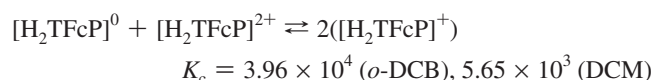(19) Barriere, F.; Geiger, W. E. *J. Am. Chem. Soc.* **2006**, *128*, 3980.
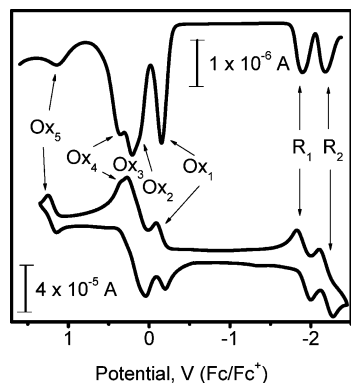
Figure 2. DPV (top) and CV (bottom) results of H_2TFcP in an *o*-DCB/TFAB system.

square-wave voltammetry (SWV) methods using low-polarity solvents (*o*-DCB and DCM) and a weakly coordinating TFAB electrolyte, with the CV and DPV results obtained in *o*-DCB shown in Figure 2. In both solvents, five reversible oxidation and two reversible reduction processes were observed (Figure 2, Table 1). Taking into consideration the relative stability of ferrocene substituents toward reduction, both reduction waves in H_2TFcP found at ~-2.2 and ~-1.9 V were assigned to the first and second reductions centered on the porphyrin macrocycle similar to those observed for numerous *meso*-aryl-substituted metal-free porphyrins.[20] The first reduction potential in H_2TFcP is more negative as compared to that of the metal-free tetraphenylporphyrin (H_2TPP), suggesting a larger electron-donating effect of the ferrocenyl substituents as compared to the phenyl groups on the porphyrin skeleton. The separation of the first and second reduction waves is similar to that of other metal-free tetraarylporphyrins.[20] For all cases studied, all reduction processes are fully reversible under CV, DPV, and SWV experimental conditions.

On the basis of spectroelectrochemical and chemical oxidation data and their potentials,[21] the first four closely spaced oxidations observed in H_2TFcP can be clearly attributed to four successful single-electron oxidations of ferrocene substituents. The $\Delta E_{1/2}$ difference between the first and second oxidation waves was found to be between 220 (DCM) and 270 (*o*-DCB) mV, the $\Delta E_{1/2}$ difference between the second and third oxidation waves was 90 mV (DCM and *o*-DCB), and that between the third and fourth oxidation waves was found to be 100 (DCM) and 180 (*o*-DCB) mV (Table 1). In each case, it was found that Ox_1-Ox_4 oxidations are close to single-electron processes, in agreement with their tentative assignment as well as spectroelectrochemical and chemical oxidation experiments, although it is extremely difficult to accurately estimate the number of electrons transferred in Ox_2 and Ox_3 processes because of their close proximity. Electrochemical data suggest the possibility of formation of several MV states in H_2TFcP despite its conformational flexibility confirmed by VT-NMR data.[8,9] The fifth oxidation process can be attributed to the removal of a single electron

from the porphyrin core. Another interesting question, which originated from electrochemical data, is the nature of the $[H_2TFcP]^{2+}$ complex. Indeed, the localization (as shown below, all spectroscopic and electrochemical data are suggestive of spin localization in all the MV $[H_2TFcP]^{n+}$ complexes) of the ferric and ferrous centers in MV $[H_2TFcP]^+$ and $[H_2TFcP]^{3+}$ can be easily assigned, while removal of an electron from $[H_2TFcP]^+$ can result in formation of $[H_2(5,10\text{-}Fc^+_2)(15,20\text{-}Fc_2)P]^{2+}$ (adjacent isomer) or $[H_2(5,15\text{-}Fc^+_2)(10,20\text{-}Fc_2)P]^{2+}$ (opposite isomer) complexes. It has been suggested[22] that the opposite isomer of $[\{(\eta^5\text{-}C_5H_5)Fe(\eta^5\text{-}C_5H_4)\}_4(\eta^4\text{-}C_4)Co(\eta^5\text{-}C_5H_5)]^{2+}$ should have a lower energy as compared to the adjacent isomer on the basis of the electrostatic repulsion between ferrocenium substituents. Such electrostatic repulsion in $[H_2TFcP]^{2+}$, however, should be small because of the large distances among ferrocene substituents, although one might speculate that the large separation between the first and the second oxidation waves is indicative of formation of the "opposite" isomer in which the largest separation between ferrocenium substituents can be achieved. Since both metal-free 5,10-bisferrocenyl-15,20-diphenylporphyrin and 5,15-bisferrocenyl-10,20-diphenylporphyrin can form MV compounds,[23] at this point it is not clear which isomer (adjacent or opposite) prevails in $[H_2TFcP]^{2+}$. The presence of the predominantly ferrocene-centered redox-active MOs (predicted by DFT) located between predominantly porphyrin-centered π and π^* MOs of H_2TFcP[8] leads to an anomalously large porphyrin ring reduction−porphyrin ring oxidation energy gap, as compared to those of the other tetraarylporphyrins. Indeed, in the majority of *meso*-tetraarylporphyrins, the first porphyrin-based oxidation and reduction are separated by ~2.4 V ("Kadish's rule"),[24] while these redox processes in H_2TFcP are separated by ~3.1 V.

The comproportionation constants (K_c) for the ferrocene-based oxidations can be easily obtained from the $\Delta E_{1/2}$ values following a well-defined procedure.[25] The calculated K_c values for H_2TFcP in *o*-DCB (DCM)/TFAB systems are

$$[H_2TFcP]^0 + [H_2TFcP]^{2+} \rightleftharpoons 2([H_2TFcP]^+)$$
$$K_c = 3.96 \times 10^4 \text{ (}o\text{-DCB)}, \ 5.65 \times 10^3 \text{ (DCM)}$$

$$[H_2TFcP]^+ + [H_2TFcP]^{3+} \rightleftharpoons 2([H_2TFcP]^{2+})$$
$$K_c = 33 \text{ (}o\text{-DCB, DCM)}$$

$$[H_2TFcP]^{2+} + [H_2TFcP]^{4+} \rightleftharpoons 2([H_2TFcP]^{3+})$$
$$K_c = 1.10 \times 10^3 \text{ (}o\text{-DCB)}, \ 49 \text{ (DCM)}$$

The large K_c of $[H_2TFcP]^+$ indicates the stability of the species, which is in agreement with the number of chemical oxidants that can produce this MV monocation. The smaller K_c values of $[H_2TFcP]^{2+}$ and $[H_2TFcP]^{3+}$ imply the relative difficulty in isolating these MV cations.

(20) (a) Kadish, K. M.; Morrison, M. M. *J. Am. Chem. Soc.* **1976**, *98*, 3326. (b) Kadish, K. M.; Caemelbecke, E. V.; Royal, G. In *Porphyrin Handbook*; Kadish, K. M., Smith, K. M., Guilard, R., Eds.; Academic Press: New York, 2000; Vol. 8, pp 1−114.

(21) (a) Geiger, W. E.; Connelly, N. G. *Adv. Organomet. Chem.* **1985**, *24*, 87. (b) Nemykin, V. N.; Maximov, A. Y.; Koposov, A. Y. *Organometallics* **2007**, *26*, 3138. (c) Nemykin, V. N.; Makarova, E. A.; Grosland, J. O.; Hadt, R. G.; Koposov, A. Y. *Inorg. Chem.* **2007**, *46*, 9591. (d) Molina, P.; Tárraga, A.; Caballero, A. *Eur. J. Inorg. Chem.* **2008**, 3401.

(22) Jiao, J.; Long, G. J.; Rebbouh, L.; Grandjean, F.; Beatty, A. M.; Fehlner, T. P. *J. Am. Chem. Soc.* **2005**, *127*, 17819.

(23) Rohde, G. T. M.S. Thesis, University of Minnesota−Duluth, 2009; 101 pp. The redox properties of metal-free 5-ferrocenyl-10,15,20-triphenylporphyrin, 5,10-bisferrocenyl-15,20-diphenylporphyrin, 5,15-bisferrocenyl-10,20-diphenylporphyrin, and 5,10,15-trisferrocenyl-20-phenylporphyrin will be published elsewhere (Nemykin, V. N.; Rohde, G. T.; Barrett, C. D.; Hadt, R. G.; Reina, G.; Galloni, P.; Floris, B. Manuscript in preparation).

(24) Kadish, K. M. *Prog. Inorg. Chem.* **1986**, *34*, 435.

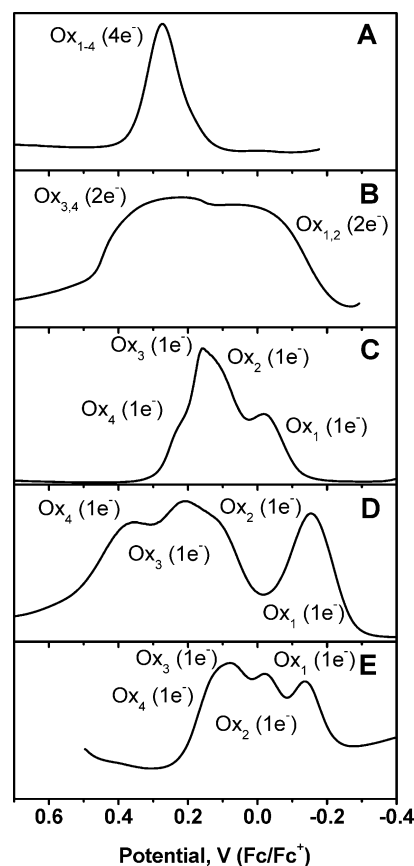(25) D'Alessandro, D.; Keene, R. *Chem. Soc. Rev.* **2006**, *35*, 424.

Table 1. Summary of Electrochemical Data for H$_2$TFcP in Different Solvents and Electrolytes[a]

	redox process						
solvent/electrolyte	H$_2$TFcP(4−)/ H$_2$TFcP(3−)	H$_2$TFcP(3−)/ H$_2$TFcP(2−)	H$_2$TFcP(2−)/ H$_2$Fc$_3$Fc$^+$P(2−)	H$_2$Fc$_3$Fc$^+$P(2−)/ H$_2$Fc$_2$Fc$^+{}_2$P(2−)	H$_2$Fc$_2$Fc$^+{}_2$P(2−)/ H$_2$FcFc$^+{}_3$P(2−)	H$_2$FcFc$^+{}_3$P(2−)/ H$_2$Fc$^+{}_4$P(2−)	H$_2$Fc$^+{}_4$P(2−)/ H$_2$Fc$^+{}_4$P(1−)
o-DCB/TFAB	−2.18	−1.91	−0.14	0.13	0.22	0.40	1.30
DCM/TFAB	−2.06	−1.78	−0.07	0.15	0.24	0.34	1.25
(bmim)Tf$_2$N	−1.60	−1.31	−0.16	−0.04	0.06	0.08	0.91
DCM/TBAP	−2.00	−1.71	−0.01	0.08	0.14	0.25	1.03
o-DCB/TBAP	−2.10	−1.86	−0.10		0.03		0.63
MeCN/TBAP	ND	ND		0.28			ND
THF/TBAP	ND	ND		0.34			ND
DMF/TBAP	ND	ND		0.32			ND

[a] Redox potentials vs (Fc/Fc$^+$). Electrolyte concentrations: TFAB, 0.05 M; TBAP, 0.10 M; (bmim)Tf$_2$N, pure liquid. ND = not determined.

Although it is possible to classify all MV cations (i.e., [H$_2$TFcP]$^+$, [H$_2$TFcP]$^{2+}$, and [H$_2$TFcP]$^{3+}$) using the calculated K_c as class II spin-localized systems, Keene, Geiger, and others[19,23,26,27] have cautioned against this method because the results are highly dependent on the polarity of the solvent and coordinating properties of the supporting electrolyte. Indeed, following Geiger's discussion,[19] when (bmim)Tf$_2$N was used as the solvent and supporting electrolyte, a quantitatively similar picture for oxidation of ferrocene substituents in H$_2$TFcP was observed, although the redox wave separation was significantly smaller (Figure 3E). The $\Delta E_{1/2}$ differences between the first and second waves, as well as the second and third waves, were ∼100 mV, while the $\Delta E_{1/2}$ difference between third and fourth oxidation waves was estimated to be ∼20 mV (Table 1). Electrochemistry in traditional DCM/TBAP yielded four separate processes for the ferrocene substituents, with the last three being closely spaced (Figure 3C, Table 1). Oxidation of the four ferrocene substituents in *o*-DCB in H$_2$TFcP can be viewed as two very diffuse, "two-electron" waves separated by ∼200 mV (Figure 3B, Table 1), and these diffuse waves may or may not represent the "real" two-electron processes. In all cases, the first oxidation wave was observed at a more negative potential as compared to the Fc/Fc$^+$ couple, in good agreement with the chemical oxidation data, which suggest the formation of [H$_2$TFcP]$^+$ when H$_2$TFcP was treated with [Fc]$^+$(PF$_6$)$^-$. When more polar DMF, THF, and MeCN were used with the traditional TBAP electrolyte, the oxidation of all ferrocene substituents occurred all at the same (more positive than the Fc/Fc$^+$ redox couple) potential (Figure 3A, Table 1). In agreement with electrochemical data, oxidation of H$_2$TFcP with [Fc]$^+$(PF$_6$)$^-$ was not observed in DMF. Overall, electrochemical data on H$_2$TFcP suggest a complex interplay between the polarity of the solvent and the nature of the electrolyte. In the best case scenario, all four single-electron oxidations of ferrocene substituents can be separated, making H$_2$TFcP potentially useful for application in redox-driven molecular electronic devices.

Spectroelectrochemistry of H$_2$TFcP in Low-Polarity Solvents Using TFAB as the Supporting Electrolyte. Since the best separation between the first four oxidation potentials of H$_2$TFcP was achieved in *o*-DCB (DCM)/TFAB systems, it became possible to obtain UV−vis−NIR spectroscopic signatures of [H$_2$TFcP]$^{n+}$ compounds using the spectroelectrochemical method.

(26) D'Alessandro, D. M.; Keene, F. R. *Dalton Trans.* **2004**, 3950.
(27) (a) Southard, G. E.; Curtis, M. D. *Organometallics* **2001**, *20*, 508. (b) Yang, J.; Seneviratne, D.; Arbatin, G.; Andersson, A. M.; Curtis, J. C. *J. Am. Chem. Soc.* **1997**, 5329. (c) Neyhart, G. A.; Hupp, J. T.; Curtis, J. C.; Timpson, C. J.; Meyer, T. J. *J. Am. Chem. Soc.* **1996**, *118*, 3724. (d) Lau, K. W.; Hu, A. M.-H.; Yen, M. H.-J.; Fung, E. Y.; Grzybicki, S.; Matamoros, R.; Curtis, J. C. *Inorg. Chim. Acta* **1994**, *226*, 137.
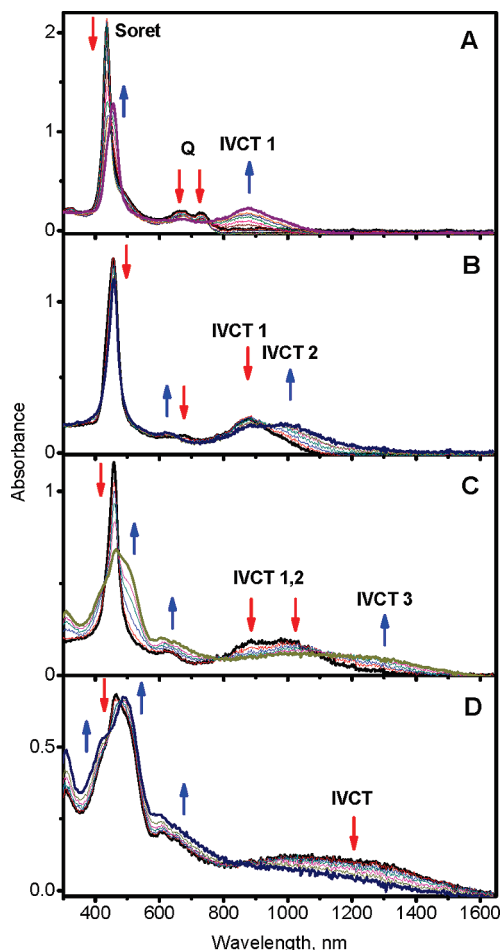
Figure 3. Comparison of DPV results of H$_2$TFcP in (A) MeCN with TBAP, (B) *o*-DCB with TBAP, (C) DCM with TBAP, (D) *o*-DCB with TFAB, and (E) (bmim)Tf$_2$N ionic liquid.

These signatures can then be used as spectroscopic benchmarks in the preparation of these compounds by a chemical oxidation.

Spectroelectrochemical oxidation of H$_2$TFcP using the *o*-DCB/TFAB system at the first oxidation potential is presented in Figure 4A. Under these conditions the Soret band, initially located at 434 nm, undergoes a red shift to 450 nm, both Q-bands decrease in intensity, and a new band located at ∼600 nm appears in the UV−vis−NIR spectrum (Table 2). In addition, as expected for the MV compounds, a characteristically intense intervalence-charge-transfer (IVCT) band located in the NIR region appears at ∼900 nm in the UV−vis−NIR spectrum of [H$_2$TFcP]$^+$. The removal of the second electron results in formation of another MV complex, [H$_2$TFcP]$^{2+}$, which has a less intense Soret band in the 450 nm region as compared to that observed in [H$_2$TFcP]$^+$. In addition, the intensity of the initial IVCT band at ∼900 nm decreases, while a new IVCT band appears at ∼1050 nm, which is lower in energy as

Figure 4. Spectroelectrochemistry results of H₂TFcP in an *o*-DCB/TFAB system: (A) H₂TFcP → [H₂TFcP]⁺ transformation, (B) [H₂TFcP]⁺ → [H₂TFcP]²⁺ transformation, (C) [H₂TFcP]²⁺ → [H₂TFcP]³⁺ transformation, and (D) [H₂TFcP]³⁺ → [H₂TFcP]⁴⁺ transformation.

compared to the IVCT in [H₂TFcP]⁺ (Figure 4B). Further removal of the third electron from H₂TFcP results in a dramatic decrease of the Soret band intensity along with the appearance of a shoulder at ~500 nm associated with this transition. The intensities of both IVCT bands (~900 and ~1050 nm) decrease, while a new IVCT band at ~1300 nm appears in the NIR region of the [H₂TFcP]³⁺ spectrum (Figure 4C). The IVCT bands disappear when [H₂TFcP]⁴⁺ is formed under spectroelectro- chemical conditions; concurrently the Soret band shifts to the ~500 nm region without losing intensity and the ~618 nm band becomes more intense. The reduction of [H₂TFcP]⁴⁺ in *o*-DCB and DCM under spectroelectrochemical conditions is reversible, resulting in the formation of H₂TFcP in which the intensity of the Soret band located at 434 nm is almost the same as that observed prior to the spectroelectrochemical experiments. Overall, spectroelectrochemical experiments generate the spec- troscopic signatures of three MV cations ([H₂TFcP]⁺, [H₂TFcP]²⁺, and [H₂TFcP]³⁺), which have a characteristic IVCT band in the NIR region of UV−vis−NIR spectra. Each further successful removal of the electron from the MV complexes results in a low-energy shift of the IVCT band. Band analysis allows for the determination of the degree of electron delocal- ization in these compounds using the Hush formalism described in the following section.

Chemical Oxidation of H₂TFcP. UV−Vis−NIR and MCD Data. With UV−vis−NIR spectroscopic signatures of [H₂TFcP]⁺, [H₂TFcP]²⁺, [H₂TFcP]³⁺, and [H₂TFcP]⁴⁺ obtained

Table 2. UV−Vis−NIR Spectral Data of H₂TFcP and [H₂TFcP]ⁿ⁺

oxidant	compound	λ_{max}, nm (log ε)[e]
none[a]	H₂TFcP	434 (5.08), 485 sh, 661 (4.24), 726 (4.18)
CCl₃CO₂H/O₂[a]	[H₂TFcP]⁺	368 (4.31), 457 (5.09), 591 (4.01), 898 (4.78)
CH₃CO₂H/O₂[a]	[H₂TFcP]⁺	366 (4.22), 456 (5.02), 591 (3.90), 890 (4.39)
CH₃CO₂H/O₂[b]	[H₂TFcP]⁺	374 (4.34), 456 (5.18), 604 (4.08), 917 (4.49)
TCNE[a]	[H₂TFcP]⁺	383 (4.33), 457 (5.16), 614 (4.05), 953 (4.48)
DDQ[a]	[H₂TFcP]⁺	455 (4.89), 581 (4.03), 933 (4.16)
[Fc]⁺(PF₆)⁻ [a]	[H₂TFcP]⁺	382 (4.42), 455 (5.14), 619 (4.20), 955 (4.45)
[Fc]⁺(PF₆)⁻ [a,c]	[H₂TFcP]⁺	381 (4.41), 457 (5.10), 609 (4.10), 944 (4.45)
[Fc]⁺(PF₆)⁻ [a,d]	[H₂TFcP]⁺	383 (4.48), 456 (5.09), 618 (4.17), 937 (4.43)
CF₃CO₂H/O₂[a]	[H₂TFcP]⁺	374 (4.30), 456 (5.15), 606 (4.08), 928 (4.50)
[NO]⁺(BF₄)⁻ [a]	[H₂TFcP]⁺	374 (4.30), 456 (5.12), 602 (4.03), 920 (4.50)
AgOTf[a]	[H₂TFcP]⁺	370 (4.30), 456 (5.04), 572, 752 (4.14), 923 (4.23)
CF₃CO₂H/O₂[a]	[H₂TFcP]²⁺	460 (4.76), 516 sh, 620 (4.14), 1188 (4.41)
AgOTf[a]	[H₂TFcP]²⁺	364 sh, 450 (4.87), 748 (4.16), 1194 (4.19)
CCl₃CO₂H/O₂[a]	[H₂TFcP]⁴⁺	368 sh, 457 (4.65), 660 (4.15), 850 sh
CCl₃CO₂H/O₂[b]	[H₂TFcP]⁴⁺	358 (4.36), 455 (4.74), 657 (4.43), 820 sh
CH₃CO₂H/O₂[b]	[H₂TFcP]⁴⁺	360 (4.36), 454 (4.76), 655 (4.46), 824 sh
DDQ[a]	[H₂TFcP]⁴⁺	459 (4.50), 669 (4.24), 870 sh

[a] Solvent DCM. [b] Solvent acetic acid. [c] Electrolyte TBAP. [d] Electrolyte TFAB. [e] sh = shoulder.

from spectroelectrochemical experiments, it is possible to follow the chemical oxidation of H₂TFcP. For instance, chemical oxidation of H₂TFcP by an appropriate oxidant (TCNE, CH₃CO₂H/ O₂,[28] DDQ, [Fc]⁺(PF₆)⁻, AgOTf,[29] I₂, or [NO]⁺[BF₄]⁻) leads to changes in the UV−vis−NIR spectra (Figure 5A) similar to those observed for the spectroelectrochemical formation of [H₂TFcP]⁺ (Figure 4A). Specifically, the Soret band shifts from 434 to 457 nm, Q-bands at 661 and 726 nm disappear, and two new bands at 591 and 898 nm appear in the UV−vis−NIR spectrum. The spectral transformation of H₂TFcP into [H₂TFcP]⁺ was further monitored by MCD spectroscopy (Figure 6A,B). The Soret band was observed as a Faraday pseudo A-term (true Faraday A-terms cannot be observed for C₂- symmetry H₂TFcP and C₁-symmetry [H₂TFcP]⁺) centered at 436 nm in H₂TFcP and upon one-electron oxidation shifts to a Faraday pseudo A-term centered at 458 nm. The initial Faraday B-terms at 670 (positive component) and 727 (negative com- ponent) nm disappear, and a new positive Faraday B-term at 605 nm appears. The IVCT band is observed as a Faraday pseudo A-term with a negative component observed at lower energy and centered at 867 nm in the spectrum (Figure 6B). The energy of the IVCT band is close to that observed in the

(28) It has been suggested (Castagnola, M.; Floris, B.; Illuminati, G.; Ortaggi, G. *J. Organomet. Chem.* **1973**, *60*, C17) that trichloro-and trifluoroacetic acids can be reduced by ferrocene into the respective aldehydes in the absence of oxygen. Thus, both oxygen and these strong acids can participate in the oxidation of H₂TFcP. Internal protonation of the porphyrin core nitrogen atoms is expected and has been observed by XPS spectroscopy. A red shift of the Soret band similar to that of oxidation is observed due to internal protonation; however, this should not lead to the formation of IVCT bands and Fe^III centers as was seen by Mössbauer and XPS spectroscopies discussed in the text.

(29) The APCI spectrum of H₂TFcP oxidized by AgOTf suggests negligible metalation of the macrocycle.
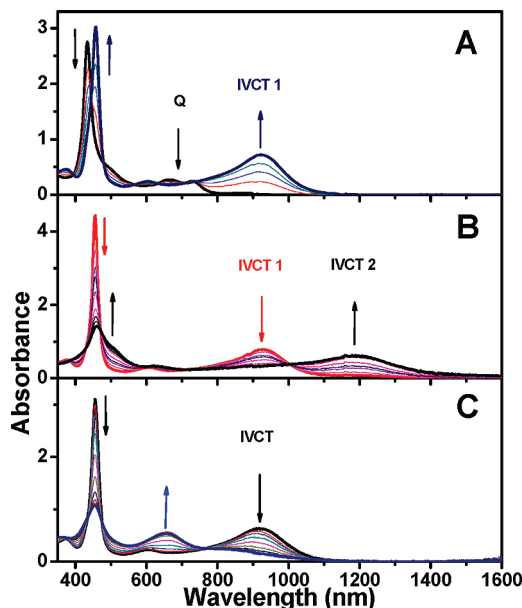
Figure 5. (A) Formation of $[H_2TFcP]^+$ by oxidation with $[NO]^+(BF_4)^-$ (0−1.1 equiv) in DCM. (B) Formation of $[H_2TFcP]^{2+}$ by oxidation with CF_3CO_2H (5 equiv)/O_2. (C) Formation of $[H_2TFcP]^{4+}$ by oxidation of $[H_2TFcP]^+$ with CF_3CO_2H (100 equiv)/O_2 in acetic acid. In all cases, spectra were taken in 5 min intervals.

MV state of metal-free octa-β-alkyl-5,15-bisferrocenylporphyrin.[5] Accurate chemical oxidation of H_2TFcP reveals seven isosbestic points in the UV−vis−NIR spectrum (Figure 5A). The position of the IVCT band in $[H_2TFcP]^+$ depends on the nature of the solvent and counterion, which is typical for the class II (in Robin−Day classification) MV compounds (Table 2). For instance, IVCT was observed at ∼880 nm in o-DCB/TFAB, while it is located at ∼920 nm in DCM; these observations are in good agreement with the other spectroscopic data indicative of the spin localization in $[H_2TFcP]^+$.

Smooth transformation of $[H_2TFcP]^+$ into MV $[H_2TFcP]^{2+}$ can be achieved either by the accurate titration of H_2TFcP in DCM with 2 equiv of AgOTf or by oxygen oxidation in the presence of 5 equiv of trifluoro- or trichloroacetic acid[28] (Figure 5B). In all cases, after transformation of the initial complex into MV $[H_2TFcP]^+$, the intensity of the Soret band decreases and shifts to 450 nm with a shoulder at ∼525 nm, the IVCT band observed at ∼900 nm decreases, and a new IVCT band at ∼1195 nm appears, in addition to the growth of a band located at ∼750 nm in UV−vis−NIR spectra, which is indicative of the formation of $[H_2TFcP]^{2+}$. The MCD spectrum of $[H_2TFcP]^{2+}$ reveals four Faraday pseudo A-terms corresponding to the main UV−vis−NIR peaks located at ∼1200, ∼730, ∼540, and ∼450 nm (Figure 6C). All of our attempts to prepare MV $[H_2TFcP]^{3+}$ failed, which is not surprising taking into consideration the small difference between the third and fourth oxidation waves in H_2TFcP. The preparation of $[H_2TFcP]^{4+}$ can be achieved by oxidation of $[H_2TFcP]^+$ in acetic acid/trichloro- or trifluoroacetic acid media[28] (Figure 5C). In UV−vis−NIR spectra, the formation of $[H_2TFcP]^{4+}$ is preceded by a dramatic decrease and significant broadening of the Soret band along with the disappearance of all IVCT bands and formation of an intense band at 657 nm, which can be assigned to the LMCT band of ferrocenium substituents (Figure 5C). The key feature in the MCD spectrum of $[H_2TFcP]^{4+}$ is the presence of a *negative* Faraday pseudo A-term, which corresponds to the Soret band in the UV−vis−NIR spectrum (Figure 6D). Again, similarly

to spectroelectrochemical experiments, the chemical oxidation of H_2TFcP is completely reversible; $[H_2TFcP]^+$, $[H_2TFcP]^{2+}$, and $[H_2TFcP]^{4+}$ can be reduced by mild reducing agents to H_2TFcP (Supporting Information Figure 2).

Traditionally, the Hush method for analysis of the experimental data is used for the evaluation of the H_{ab} coupling element by the majority of synthetic chemists.[30] A more descriptive analysis of the intramolecular-electron-transfer characteristics in MV compounds, however, requires an intimate familiarization with the variation of the electronic energy as a function of the nuclear coordinates.[23,31] For instance, Piepho, Krausz, and Schatz[32] and Ondrechen and co-workers[33] have developed models to analyze the MV dynamics in the Creutz−Taube ion.[34] Piepho's molecular-orbital-based method[35] has also been used.

H_{ab} and α, the electronic coupling matrix element and delocalization parameter, respectively, can be estimated using eqs 1 and 2, and DFT-predicted Fe−Fe distances in H_2TFcP, and are displayed in Table 3.[23,27,36]

$$H_{ab} = (2.05 \times 10^{-2})\frac{(\nu_{max}\varepsilon_{max}\Delta\nu_{1/2})^{1/2}}{r_{ab}} \quad (1)$$

$$\alpha = (4.2 \times 10^{-4})\frac{\Delta\nu_{1/2}\varepsilon_{max}}{\nu_{max}r_{ab}^2} \quad (2)$$

where ν_{max} is the energy of the IVCT at the band maximum (cm^{-1}), $\Delta\nu_{1/2}$ is the half-width at the band maximum (cm^{-1}), ε_{max} is the molar extinction coefficient of the IVCT, and r_{ab} is the distance between redox centers (Å).

Although H_{ab} and α values for the MV $[H_2TFcP]^+$, $[H_2TFcP]^{2+}$, and $[H_2TFcP]^{3+}$ complexes are considered as crude estimates, several trends can be seen. First, the values of H_{ab} gradually decrease upon stepwise oxidation of H_2TFcP under the same reaction conditions. Second, the magnitude of the estimated values of α put $[H_2TFcP]^+$, $[H_2TFcP]^{2+}$, and $[H_2TFcP]^{3+}$ into class II (spin-localized) systems in the Robin and Day classification scheme.[37] The spin-localized classification is in excellent agreement with the other spectroscopic evidence presented below. Finally, the magnitudes of H_{ab} ($H_{ab} \approx 0.1\nu_{max}$) are also in good agreement with the class II classification, although the H_{ab} and α values (Table 3) can only be treated as a crude estimation as is well-discussed in the literature.[28,38]

^{57}Fe Mössbauer Spectroscopy. Temperature-dependent Mössbauer studies on MV biferrocenium systems provided a unique opportunity to study the influence of crystal packing forces and types of counterions on the thermal dependency of the intramolecular-electron-transfer process.[4j] In the majority of complexes, class II behavior dominates, resulting in the observation of individual ferrocene (large quadrupole splitting doublet) and

(30) Hush, N. S. *Prog. Inorg. Chem.* **1967**, *8*, 391.
(31) (a) Brunschwig, B. S.; Sutin, N. *Coord. Chem. Rev.* **1999**, *187*, 233. (b) Brunschwig, B. S.; Creutz, C.; Sutin, N. *Chem. Soc. Rev.* **2002**, *31*, 168.
(32) (a) Piepho, S. B.; Krausz, E. R.; Schatz, P. N. *J. Am. Chem. Soc.* **1978**, *100*, 2996. (b) Wong, K. Y.; Schatz, P. N. *Prog. Inorg. Chem.* **1981**, *28*, 369.
(33) Zhang, L.-T.; Ko, J.; Ondrechen, M. J. *J. Am. Chem. Soc.* **1987**, *109*, 1666.
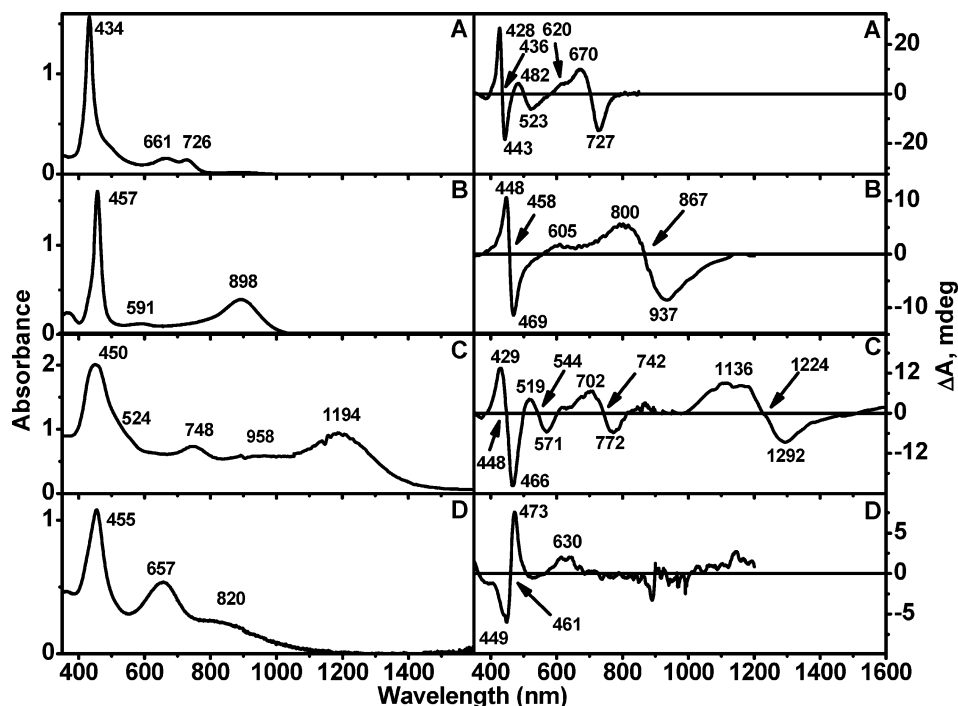(34) Creutz, C.; Taube, H. *J. Am. Chem. Soc.* **1969**, *91*, 3988.
(35) Piepho, S. B. *J. Am. Chem. Soc.* **1988**, *110*, 6319.
(36) Lever, A. B. P. *Inorganic Electronic Spectroscopy*, 2nd ed.; Elsevier: Amsterdam, 1984; p 612.
(37) Creutz, C. *Prog. Inorg. Chem.* **1983**, *30*, 1.
(38) D'Alessandro, D.; Keene, R. *Chem. Rev.* **2006**, *106*, 2270.

Figure 6. Absorbance (left) and MCD (right) results of H_2TFcP (A), $[H_2TFcP]^+$ (B), $[H_2TFcP]^{2+}$ (C), and $[H_2TFcP]^{4+}$ (D) in DCM (A−C) or acetic acid (D).

Table 3. Estimated Magnitudes of H_{ab} and α for Mixed-Valence $[H_2TFcP]^{n+}$ Complexes[a]

compound/oxidant	IVCT ν_{max}, cm^{-1}	ε_{max}, M^{-1} L^{-1}	$\Delta\nu_{1/2}$, cm^{-1}	r_{ab}, Å	H_{ab}, cm^{-1}	$\alpha \times 10^3$
$[H_2TFcP]^+$	10760	31875	855	9.83	1135	11.14
CH_3CO_2H/O_2				9.76	1143	11.30
$[H_2TFcP]^+$	10600	17750	621	9.83	716	4.57
AgOTf				9.76	721	4.64
$[H_2TFcP]^+$	10900	28405	960	9.83	1143	11.00
DDQ				9.76	1151	11.16
$[H_2TFcP]^+$	10420	29165	758	9.83	1006	9.33
TCNE				9.76	1013	9.47
$[H_2TFcP]^+$	11065	21218	876	9.83	950	7.39
e-chem				9.76	957	7.50
$[H_2TFcP]^+$	10775	33305	795	9.83	1119	10.81
CF_3CO_2H/O_2				9.76	1127	10.96
$[H_2TFcP]^{2+}$	8400	16260	685	9.83	641	5.83
AgOTf				9.76	646	5.92
$[H_2TFcP]^{2+}$	8350	25595	598	9.83	749	8.06
CF_3CO_2H/O_2				9.76	755	8.18
$[H_2TFcP]^{2+}$	9770	16050	873	9.83	775	6.31
e-chem				9.76	781	6.40
$[H_2TFcP]^{3+}$	7914	10880	820	9.83	557	4.96
e-chem				9.76	561	5.03

[a] Fe−Fe (r_{ab}) distances are taken from the DFT-optimized structure of H_2TFcP and represent the closest Fe−Fe distances.[8]

Table 4. Mössbauer Data on H_2TFcP and $[H_2TFcP]^{n+}$ Complexes

sample/oxidant	T, K	Fe^{II} δ^a	Fe^{II} ΔE_Q	Fe^{III} δ^a	Fe^{III} ΔE_Q	Fe^{IIb}	Fe^{IIIb}
H_2TFcP	90	0.517	2.362			4 (100)	0
$[H_2TFcP]^+(CH_3CO_2)^-$	96.5	0.518	2.316	0.494	0.484	3 (73)	1 (27)
$[H_2TFcP]^+(CH_3CO_2)^-$	302	0.441	2.311	0.371	0.644	3 (76)	1 (24)
$[H_2TFcP]^+(I_3)^-$	96.2	0.489	1.890	0.520	0.252	3 (72)	1 (28)
$[H_2TFcP]^+(DDQ)^-$	94	0.535	2.291	0.537	0.253	3 (71)	1 (29)
$[H_2TFcP]^{2+}\cdot 2(DDQ)^-$	95	0.530	2.011	0.455	0.425	2 (48)	2 (52)
$[H_2TFcP]^{2+}\cdot 2(DDQ)^-$	96.6	0.534	2.150	0.494	0.770	2 (48)	2 (52)
$[H_2TFcP]^{2+}\cdot 2(CCl_3CO_2)^-$	96.5	0.545	2.261	0.496	0.601	2 (44)	2 (56)
$[H_2TFcP]^{2+}\cdot 2(I_3)^-$	93.2	0.533	1.933	0.463	0.742	2 (52)	2 (48)
$[H_2TFcP]^{4+}\cdot 4(CCl_3CO_2)^-$	92.4			0.535	0.734	0	4 (100)^c
$[H_2TFcP]^{4+}\cdot 4(CCl_3CO_2)^-$	291			0.461	0.674	0	4 (100)^c

[a] The isomer shifts are relative to α-Fe; the typical uncertainty for measurements is ±0.003 mm/s. [b] Iron atoms assigned (area percentage). [c] Contains ∼5% high-spin Fe^{II} impurity originated from tap water used to wash the sample.

H_2TFcP results in the formation of MV $[H_2TFcP]^+$, which can be characterized by two doublets in the Mössbauer spectrum, which are characteristic for spin-trapped, MV compounds (Table 4, Figure 7B). For instance, in the $[H_2TFcP]^+(DDQ)^-$ complex, the ferrocene centers are represented by the major doublet with an isomer shift of 0.54 mm/s and quadrupole splitting of 2.29 mm/s, while the ferrocenium substituent is represented by the minor Mössbauer doublet with an isomer shift of 0.54 mm/s and quadrupole splitting of 0.25 mm/s. To investigate possible electron delocalization at elevated temperatures previously known for polyferrocenyl-containing compounds, two samples of $[H_2TFcP]^+$ were tested in the 90−300 K range. At all temperatures, only two doublets were observed in the Mössbauer

ferrocenium (small quadrupole splitting doublet) Mössbauer signals. In several cases, however, the barrier to thermal electron transfer was lowered as a result of cation−anion interactions and/or packing forces, and as a result, the high-temperature Mössbauer spectrum consists of a single "average-valence" doublet, suggesting a fast ($\sim 10^{-7}$ s) thermal electron-transfer rate between Fe^{II} and Fe^{III} centers.[39] The ^{57}Fe Mössbauer spectrum of H_2TFcP consists of a single doublet (Table 4, Figure 7A) with an almost temperature-independent large quadrupole splitting of 2.362 mm/s and an isomer shift of 0.517 mm/s (90 K) which is characteristic for diamagnetic Fe^{II} low-spin ferrocene-containing compounds.[40] Single-electron oxidation of

(39) Gütlich, P.; Ensling, J. In *Inorganic Electronic Structure and Spectroscopy*; Lever, A. B. P., Solomon, E. I., Eds.; John Wiley & Sons: New York, 1999; Vol. I, p 161.

(40) (a) Venkatasubbaiah, K.; Doshi, A.; Nowik, I.; Herber, R. H.; Rheingold, A. L.; Jäkle, F. *Chem.—Eur. J.* **2008**, *14*, 444. (b) Webb, R. J.; Geib, S. J.; Staley, D. L.; Rheingold, A. L.; Hendrickson, D. N. *J. Am. Chem. Soc.* **1990**, *112*, 5031. (c) Kaufmann, L.; Breunig, J.-M.; Vitze, H.; Schoedel, F.; Nowik, I.; Pichlmaier, M.; Bolte, M.; Lerner, H.-W.; Winter, R. F.; Herber, R. H.; Wagner, M. *Dalton Trans.* **2009**, 2940. (d) Herber, R. H.; Nowik, I. *J. Organomet. Chem.* **2008**, *693*, 3007. (e) Nowik, I.; Herber, R. H. *Eur. J. Inorg. Chem.* **2006**, 5069.
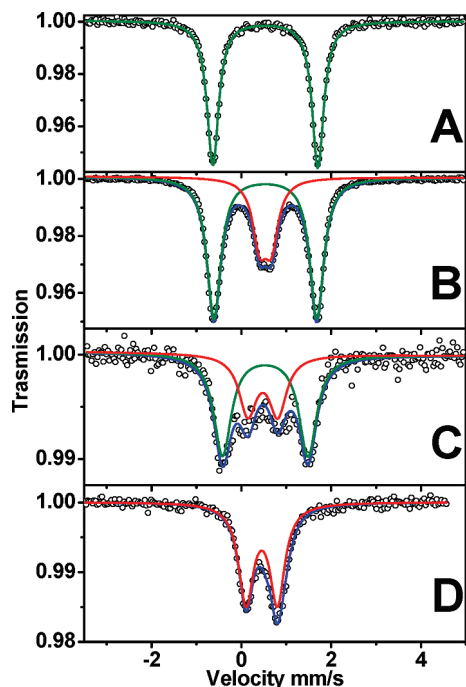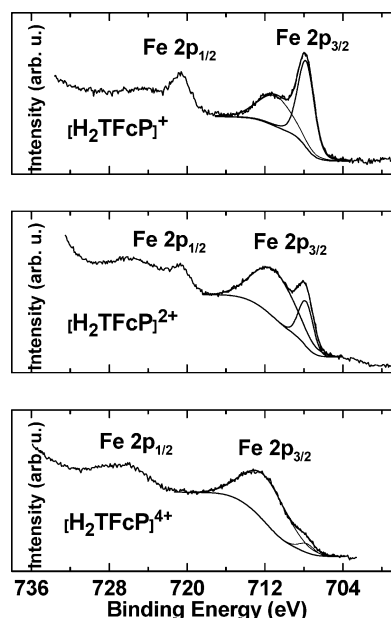
Figure 7. Mössbauer spectra (90 K) of H₂TFcP (A), [H₂TFcP]⁺(DDQ)⁻ (B), [H₂TFcP]²⁺·2(DDQ)⁻ (C), and [H₂TFcP]⁴⁺·4(CCl₃CO₂)⁻ (D).

Figure 8. Experimental and theoretically reconstructed Fe 2p XPS spectra for [H₂TFcP]⁺(DDQ)⁻, [H₂TFcP]²⁺·2(CCl₃CO₂)⁻, and [H₂TFcP]⁴⁺·4(CCl₃CO₂)⁻.

spectra of [H₂TFcP]⁺, suggesting that the spin-trapped behavior remains intact over a large range of temperatures. In all cases studied at low temperatures (∼90 K), the ratio between ferrocene Fe^{II} and ferrocenium Fe^{III} doublets is close to that expected for [H₂TFcP]⁺, 3:1, and only a minor temperature dependence of the quadrupole splittings and Mössbauer absorption fraction was observed for both doublets.[41] The quadrupole splitting of the ferrocenium doublet has slight counterion dependence and varies between 0.25 and 0.64 mm/s. Two distinct doublets, which are characteristic for spin-trapped MV complexes, are also observed in the ^{57}Fe Mössbauer spectra of [H₂TFcP]²⁺ over a large temperature range (Table 4, Figure 7C). The counterion dependence of the quadrupole splitting parameter in [H₂TFcP]²⁺ is less prominent as compared to that found in [H₂TFcP]⁺ (Table 4). Again, the ratio of ferrocene to ferrocenium centers is close to the expected 1:1, while a nonperfect area ratio can be explained on the basis of the difference of the well-known different probabilities of recoil free absorption of Fe^{II} and Fe^{III} centers. Finally, a single almost temperature-independent doublet (δ = 0.53 mm/s, ΔE_Q = 0.73 mm/s) characteristic of the ferrocenium ions is observed in the Mössbauer spectrum of [H₂TFcP]⁴⁺ (Table 4, Figure 7D). Thus, overall, both [H₂TFcP]⁺ and [H₂TFcP]²⁺ MV complexes behave as spin-localized valence-trapped systems on the Mössbauer time scale of 10^{-7} s⁻¹, and this behavior remains intact over the large range of temperatures, suggesting that the thermal electron transfer barrier in these class II MV compounds is larger than the magnitude of kT.[42]

XPS Spectra. XPS spectra of polynuclear transition-metal complexes have been used for the possible identification of spin localization in the electronic ground state of complex MV

ruthenium and iron compounds.[43] The time scale of XPS is significantly shorter (∼10^{-16} s) relative to that of Mössbauer spectroscopy (10^{-7} s), and systems which are spin-localized in Mössbauer experiments should be seen as spin-localized systems also in XPS experiments. The photoemission process, however, leaves the system in an ionized state, and relaxation events which can accompany the primary process can complicate the interpretation of XPS spectra in terms of the ground state of the system. XPS spectra of [H₂TFcP]⁺, [H₂TFcP]²⁺, and [H₂TFcP]⁴⁺ in the Fe 2p region are shown in Figure 8, and demonstrate a stepwise oxidation of ferrocene into ferrocenium centers. As expected, in the case of the H₂TFcP complex,[8] only Fe^{II} centers are present in the XPS Fe 2p region, as inferred from the binding energy of the Fe 2p$_{3/2}$ peak (∼708 eV) and its associated narrow full width (∼2 eV). Similarly, one Fe 2p$_{3/2}$ peak located at ∼712−713 eV with the characteristic Fe^{III} complex line shape due to shake-up satellite lines, was observed in the XPS spectrum of [H₂TFcP]⁴⁺ (with only a very small Fe^{II} component at ∼708 eV likely due to some decomposition under X-ray irradiation), confirming oxidation of all iron centers. In the three compounds, the experimental N:Fe atomic ratio equals the theoretically expected value. In excellent agreement with results from Mössbauer spectroscopy, XPS spectra of the MV [H₂TFcP]⁺ and [H₂TFcP]²⁺ complexes in the Fe 2p region consist of two signals characteristic for ferrocene and ferrocenium centers with close to the expected 3:1 and 1:1 ratios. Thus, also XPS data are consistent with spin localization in the MV [H₂TFcP]⁺ and [H₂TFcP]²⁺ complexes.

IR Spectra. IR spectroscopy in the 500−1000 cm⁻¹ range can be used as a probe for electron localization in a variety of MV complexes including polyferrocenyl-containing compounds.[22,41] Specifically, the frequency of the C−H bending vibration can be used as one of the most characteristic fingerprints for ferrocene to ferrocenium oxidation. Indeed, the former one is located at ∼815 cm⁻¹, while the latter is observed at ∼850 cm⁻¹.

(41) Jiao, J.; Long, G. J.; Grandjean, F.; Beatty, A. M.; Fehlner, T. P. *J. Am. Chem. Soc.* **2003**, *125*, 7522.
(42) Kramer, J. A.; Hendrickson, D. N. *Inorg. Chem.* **1980**, *19*, 3330.

(43) (a) Citrin, P. H.; Ginsberg, A. P. *J. Am. Chem. Soc.* **1981**, *103*, 3673. (b) Chakraborty, I.; Baran, P.; Sanakis, Y.; Simopoulos, A.; Fachini, E.; Raptis, R. G. *Inorg. Chem.* **2008**, *47*, 11734.
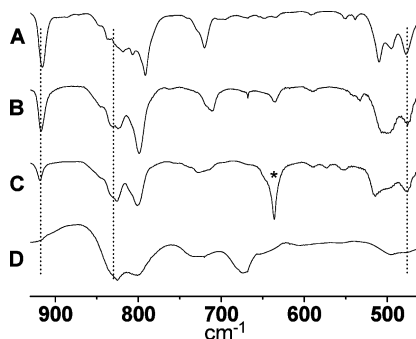
Figure 9. Solid-state (KBr pellets) IR spectra of H₂TFcP (A), $[H_2TFcP]^+$·(CCl₃CO₂)⁻ (B), $[H_2TFcP]^{2+}$·2(OTf)⁻ (C), and $[H_2TFcP]^{4+}$·4(CCl₃CO₂)⁻ (D) in the 950−450 cm⁻¹ region. The asterisk indicates the (OTf)⁻ counterion peak.

Correspondingly, in the cases when the electron-transfer rate in the MV polyferrocenyl-containing complexes is smaller than the IR time scale (10^{-12} s), the intensity of the C−H bending vibration located at ferrocene substituents decreases, while the intensity of the C−H bending vibration located at ferrocenium substituents increases upon stepwise oxidation of the parent complex.

The representative IR spectra of H₂TFcP, $[H_2TFcP]^+$, $[H_2TFcP]^{2+}$, and $[H_2TFcP]^{4+}$ are shown in Figure 9. From the IR spectrum of H₂TFcP, it is clear that there are several bands present in the 795−850 cm⁻¹ region. The analysis of the vibrational spectrum of H₂TFcP calculated at the DFT level (Supporting Information Figures 3 and 4) reveals several IR-active vibrations in this region (specifically ν_{111}, ν_{113}, ν_{115}, ν_{116}, and ν_{136}−ν_{140}), which form two intense IR bands at 789 and 822 cm⁻¹. Out of these, ν_{113} and ν_{140} are the most intense, while several ferrocene vibrations coupled to the porphyrin core have significantly smaller intensities. This situation makes it very complicated to follow the intensity of the ferrocene C−H bending vibrations. Fortunately, upon stepwise oxidation of the H₂TFcP complex, the C−H bending vibrations of ferrocenium substituents observed at 823 cm⁻¹ gain significant intensity and thus can serve as a benchmark for the formation of $[H_2TFcP]^+$, $[H_2TFcP]^{2+}$, and $[H_2TFcP]^{4+}$ compounds. In addition, ferrocene-containing modes ν_{170}, ν_{171}, ν_{174}, and ν_{175} (Supporting Information Figure 4) form a strong band predicted at 898 cm⁻¹ by DFT calculations and experimentally observed at 919 cm⁻¹. This band loses its intensity upon stepwise oxidation of the H₂TFcP complex and disappears in the $[H_2TFcP]^{4+}$ compound. Fe−Cp vibrations located at ∼500 cm⁻¹ can also be used to monitor the degreee of oxidation in H₂TFcP (Figure 9). Indeed, the intensity of the IR band observed at 477 cm⁻¹, which according to our DFT calculations consists of two closely spaced Fe−Cp ν_{76} and ν_{77} vibrations, decreases as a result of stepwise oxidation of H₂TFcP. All of these transformations suggest that the MV $[H_2TFcP]^+$ and $[H_2TFcP]^{2+}$ complexes have localized Fe^{II} and Fe^{III} ferrocene moieties on the IR time scale.

The observation of MV states in $[H_2TFcP]^+$, $[H_2TFcP]^{2+}$, and $[H_2TFcP]^{3+}$ clearly suggests that, differently from what was proposed by Barrrell et al.,[5] conformational rigidity cannot be considered as the only factor controlling the formation of MV states in polyferrocenylporphyrins, although it can affect the degree of localization/delocalization in these systems. The formation of the MV states of H₂TFcP is highly dependent on the solvents/electrolytes. The separation of four single-electron oxidation processes in a noncoordinating solvent and electrolyte allowed for the electrochemical formation of the MV complexes

$[H_2TFcP]^+$, $[H_2TFcP]^{2+}$, and $[H_2TFcP]^{3+}$ whose electronic absorption spectra match those of the MV ions ($[H_2TFcP]^+$ and $[H_2TFcP]^{2+}$) formed by chemical oxidation.

Conclusions

Redox properties of the H₂TFcP complex were investigated using CV, DPV, and SWV methods in a large variety of solvents and electrolytes. When DMF, THF, and AN were used with TBAP as the supporting electrolyte, the first oxidation wave was assigned to a four-electron oxidation process reflecting simultaneous oxidation of all iron(II) centers into iron(III) in the H₂TFcP. When the *o*-DBC/TBAP combination was used in electrochemical experiments, four ferrocene substituents underwent two very diffuse "two-electron" stepwise oxidations. Use of a weakly coordinating TFAB electrolyte in *o*-DCB or DCM resulted in four single-electron oxidation processes for the ferrocene substituents in which the first and second single-electron waves have a relatively large separation, while the third and fourth oxidation processes are closely spaced; similar results were observed with the DCM/TBAP and pure ionic liquid systems, albeit with smaller wave separation. Spectroelectrochemical oxidation of H₂TFcP in *o*-DCB or DCM with TFAB as the supporting electrolyte allowed characterization of the MV $[H_2TFcP]^+$, $[H_2TFcP]^{2+}$, and $[H_2TFcP]^{3+}$ compounds by UV−vis spectroscopy in addition to the "all-Fe^{III}" tetracation $[H_2TFcP]^{4+}$. The chemical oxidation of H₂TFcP was tested using a variety of oxidants and results in formation of MV $[H_2TFcP]^+$ and $[H_2TFcP]^{2+}$ complexes as well as $[H_2TFcP]^{4+}$, which were characterized by UV−vis, MCD, Mössbauer, FT-IR, and XPS spectroscopic methods. The intervalence-charge-transfer bands observed in the near-IR region in $[H_2TFcP]^+$ and $[H_2TFcP]^{2+}$ complexes were analyzed using the Hush formalism and are suggestive of class II (in Robin−Day classification) character with localized ferrous and ferric centers. Class II behavior of $[H_2TFcP]^+$ and $[H_2TFcP]^{2+}$ complexes was further confirmed by FT-IR, Mössbauer, and XPS data.

Experimental Section

Materials. All reactions were performed under a dry nitrogen atmosphere with flame-dried glassware. Pyrrole, ferrocenecarbaldehyde, benzaldehyde, boron trifluoride etherate, chloranil, and triethylamine were purchased from commercially available sources and used without further purification. Silica gel (60 Å, 32−63 mesh) was purchased from Sorbent Technologies, basic aluminum oxide (activity I, 58 Å, 150 mesh) was purchased from Fischer Inc., and Bio-Beads (SX-1 and SX-3) for size exclusion filtration were purchased from Bio-Rad. All solvents were dried with appropriate drying agents (molecular sieves for DMF; CaH₂ for DCM, MeCN, *o*-DCB; sodium for THF) and distilled directly prior to the experiments. 1-Butyl-3-methylimidazolium bis(trifluoromethanesulfonyl)imide, (bmim)Tf₂N, was prepared according to the literature,[44] by quaternization of 1-methylimidazole with 1-bromobutane and subsequent metathesis reaction with NaTf₂N.

Physical Measurements. UV−vis−NIR data were obtained on an HP 8453 or a Cary 17 spectrometer. MCD data were recorded using an OLIS DCM 17 CD spectropolarimeter using a 1.4 T DeSa magnet. The spectra were recorded twice for each sample, once with a parallel field and again with an antiparallel field, and their intensities were expressed by molar ellipticity per $T = [\Theta]_M/(\text{deg dm}^3 \text{ mol}^{-1} \text{ cm}^{-1} \text{ T}^{-1})$. Mössbauer spectra were recorded in constant acceleration mode. The source was ⁵⁷Co in a rhodium matrix with an initial activity of 100 mCi. The air-stable solids were ground with Pyrex powder and mixed with BN to ensure random crystallite

(44) Owens, G. S.; Abu-Omar, M. M. *J. Mol. Catal. A* **2002**, *187*, 215.

orientation in the subsequent MES measurements, transferred to Perspex sample holders, and mounted in a cryostat in transmission geometry as previously described.[45] Spectrometer calibration was effected with α-Fe, and all isomer shifts are referred to the centroid of such room temperature calibration spectra. Temperature control over the data sampling intervals (typically 8−36 h) was held to ±0.2° and monitored with the Daswin program.[46] Electrochemical measurements were conducted using a CH electrochemical analyzer utilizing a three-electrode scheme with platinum or glassy carbon working electrodes and platinum wires as auxiliary and pseudoreference electrodes. A 0.1 M solution of TBAP or 0.05 M solution of TFAB electrolyte was used with the appropriate solvent. Potentials were corrected using the internal standard decamethylferrocene in all cases except [bmim]$^+$[Tf$_2$N]$^-$, when the external standard ferrocene was used. Potentials were then corrected to ferrocene using −0.670 for Me$_{10}$Fc/Me$_{10}$Fc$^+$ vs Fc/Fc$^+$ for o-DCB/ TFAB and the following references for all others.[19,47] Spectroelectrochemical data were collected in a 0.15 M solution of TFAB in o-DCB or DCM with the oxidation potential set slightly negative of the peak being investigated. Reversibility experiments were conducted at −0.3 V potentials. The compounds were prepared for XPS measurements by grounding the solid into fine grains in an agate mortar, and homogeneously spread over a graphite sheet attached to a stainless steel XPS sample holder. Photoelectron spectra have been acquired with a modified Omicrometer NanoTechnology MXPS system equipped with a dual X-ray anode source (Omicrometer DAR 400) and an Omicrometer EA-127 hemispherical energy analyzer operated in constant analyzer energy (CAE) mode, with a pass energy of 20 eV. Al Kα ($h\nu = 1486.6$ eV) and Mg Kα ($h\nu = 1253.6$ eV) photons were used to excite photoemission, operating at 14−15 kV and 10−20 mA. Data fitting with commercially available routines was applied using linear or Shirley backgrounds and linear combinations of Lorentzian and Gaussian line shapes to determine full widths at half-maximum (fwhm) and binding energies (BEs) of the relevant core lines. The accuracy of reported BEs is ±0.2 eV, and the reproducibility of the results is within these values. XPS atomic ratios for the investigated compounds have been estimated from experimentally determined area ratios of core lines, after subtraction of the background, removal of X-ray satellite peaks (deriving from the K$\alpha_{3,4}$ components of the nonmonochromatic photon sources[48]), normalization for the atomic cross-section values, and correction for an inverse dependence of the square root of kinetic energies. Atomic ratios are associated with an error of ±15%. IR spectra were recorded in the solid state in KBr pellets using an HP 1310 instrument.

Computational Aspects. All DFT calculations were conducted using the GAUSSIAN 03 software package running under either Windows or UNIX OS.[49] The molecular geometries were optimized using Becke's three-parameter hybrid exchange functional[50] and the Lee−Yang−Parr nonlocal correlation functional[51] (B3LYP) coupled with the 6-31G(d) basis set for all atoms. For all optimized structures, frequency calculations were carried out to ensure optimized geometries represented local minima.

Syntheses. 1. Preparation of H$_2$TFcP. This complex was prepared and purified following a well-established procedure.[8,9,16]

2. Preparation of [H$_2$TFcP]$^+$(X)$^-$. In a typical procedure, [NO]$^+$(BF$_4$)$^-$ (5.6 mg, 0.048 mmol) was added to the solution of

50 mg (0.048 mmol) of H$_2$TFcP in CH$_2$Cl$_2$ (10 mL) at room temperature. The reaction mixture was stirred for 5 min, after which 20 mL of hexane was added. The [H$_2$TFcP]$^+$(BF$_4$)$^-$ precipitate was filtered, washed several times with hexane and water, and dried in vacuum. Yield: 42 mg (78%). Similarly, other [H$_2$TFcP]$^+$(X)$^-$ complexes were prepared by oxidizing H$_2$TFcP in CH$_2$Cl$_2$ with I$_2$, DDQ, CCl$_3$CO$_2$H, [Fc]$^+$(PF$_6$)$^-$, or AgOTf. In all cases, the reaction was monitored by UV−vis−NIR until the transformation of H$_2$TFcP into [H$_2$TFcP]$^+$(X)$^-$ was completed (typically 5−15 min). After this period of time, excess hexane was added, and the precipitate was filtered, washed several times with hexane and water, and dried in vacuum. Spectroscopic data for individual compounds are presented in Tables 2 and 4. Selected elemental analysis for [H$_2$TFcP]$^+$(CCl$_3$CO$_2$)$^-$·CCl$_3$CO$_2$H: Anal. Calcd for C$_{64}$H$_{44}$N$_4$- Fe$_4$Cl$_6$O$_4$: C, 56.02; H, 3.45; N, 4.08. Found: C, 56.91; H, 3.59; N, 4.84.

3. Preparation of [H$_2$TFcP]$^{2+}$·2(X)$^-$. In a typical procedure, trichloroacetic acid (31.2 mg, 0.19 mmol) was added to a solution of 50 mg (0.048 mmol) of H$_2$TFcP in CH$_2$Cl$_2$ (10 mL) at room temperature. The reaction mixture was stirred for 1 h, after which 20 mL of hexane was added. The precipitate of [H$_2$TFcP]$^{2+}$· 2(CCl$_3$CO$_2$)$^-$·CCl$_3$CO$_2$H was filtered, washed several times with hexane and water, and dried in vacuum. Yield: 63 mg (86%). Similarly, other [H$_2$TFcP]$^{2+}$·2(X)$^-$ complexes were prepared by oxidizing H$_2$TFcP in CH$_2$Cl$_2$ with 5 equiv of CF$_3$CO$_2$H or 2.2 equiv of AgOTf. In all cases, the reaction was monitored by UV−vis−NIR until the transformation of [H$_2$TFcP]$^+$ into [H$_2$TFcP]$^{2+}$·2(X)$^-$ was completed (typically 1−2 h). After this period of time, excess hexane was added, and the precipitate was filtered, washed several times with hexane and water, and dried in vacuum. Spectroscopic data for individual compounds are presented in Tables 2 and 4. Selected elemental analysis for [H$_2$TFcP]$^{2+}$·2(CCl$_3$CO$_2$)$^-$·CCl$_3$CO$_2$H: Anal. Calcd for C$_{66}$H$_{47}$N$_4$Fe$_4$Cl$_9$O$_6$: C, 51.66; H, 3.09; N, 3.65. Found: C, 51.97; H, 3.10; N, 3.51. Selected elemental analysis for [H$_2$TFcP]$^{2+}$· 2(OTf)$^-$·HOTf: Anal. Calcd for C$_{63}$H$_{47}$F$_9$N$_4$Fe$_4$O$_9$S$_3$: C, 50.63; H, 3.17; N, 3.75. Found: C, 49.94; H, 3.55; N, 3.61.

4. Preparation of [H$_2$TFcP]$^{4+}$·4(X)$^-$. In a typical procedure, trichloroacetic acid (780 mg, 4.78 mmol) was added to a solution of 50 mg (0.048 mmol) of H$_2$TFcP in acetic acid (15 mL) at room temperature. The reaction mixture was stirred for 24 h, after which 50 mL of water was added. The precipitate of [H$_2$TFcP]$^{4+}$· 4(CCl$_3$CO$_2$)$^-$·CCl$_3$CO$_2$H was filtered, washed several times with water, and dried in vacuum. Yield: 83 mg (93%). Similarly, the [H$_2$TFcP]$^{4+}$·4(CF$_3$CO$_2$)$^-$·CF$_3$CO$_2$H complex was prepared by oxidizing H$_2$TFcP in acetic acid with 100 equiv of CF$_3$CO$_2$H for 24 h. Spectroscopic data for individual compounds are presented in Tables 2 and 4. Selected elemental analysis for [H$_2$TFcP]$^+$· 4(CCl$_3$CO$_2$)$^-$·CCl$_3$CO$_2$H: Anal. Calcd for C$_{70}$H$_{47}$N$_4$Fe$_4$Cl$_{15}$O$_{10}$: C, 45.22; H, 2.55; N, 3.01. Found: C, 45.08; H, 2.69; N, 2.92.

Supporting Information Available: Chemical and electrochemical reductions of [H$_2$TFcP]$^{n+}$ into H$_2$TFcP, IR spectrum of H$_2$TFcP calculated at the DFT level and important vibrational modes discussed in the text, and full citation for ref 49. This material is available free of charge via the Internet at http:// pubs.acs.org.

JA905310H

(45) Herber, R. H.; Nowik, I.; Grossland, J. O.; Hadt, R. G.; Nemykin, V. N. *J. Organomet. Chem.* **2008**, *693*, 1850.
(46) MegaDaq Data Acquisition System Home Page. http://www.mega-daq.com (accessed Sept 16, 2009).
(47) Noviandri, I.; Brown, K. N.; Fleming, D. S.; Gulyas, P. T.; Lay, P. A.; Master, A. F.; Phillis, L. *J. Phys. Chem. B* **1999**, *103*, 6713.
(48) Briggs, D.; Seah, M. P. *Practical Surface Analysis*, 2nd ed.; J. Wiley & Sons: Chichester, U.K., 1990; Vol. 1.
(49) Frisch, M. J.; et al. *GAUSSIAN 03*, revision C.02; Gaussian, Inc.: Wallingford, CT, 2004. See the Supporting Information for the full citation.
(50) Becke, A. D. *Phys. Rev. A* **1988**, *38*, 3098.
(51) Lee, C.; Yang, W.; Parr, R. G. *Phys. Rev. B* **1988**, *37*, 785.